Soil Biology and Biochemistry 139 (2019) 107624

Contents lists available at ScienceDirect

Soil Biology and Biochemistry

journal homepage: http://www.elsevier.com/locate/soilbio

Competitor and substrate sizes and diffusion together define enzymatic depolymerization and microbial substrate uptake rates

Jinyun Tang *, William J. Riley

Climate and Ecosystem Sciences Division, Berkeley, CA, 94720, USA

ARTICLE INFO

Keywords:
Soil organic matter decomposition
Diffusion limitation
Half saturation constant
Maximum reaction rates
Enzymatic depolymerization

1-2
2 notes:

ABSTRACT

Diffusion limitations of extracellular enzymes and soluble monomers have been recognized as important mechanisms controlling soil organic matter (SOM) dynamics. Here we combine diffusion limitation with the geometric sizes of extracellular enzymes, polymer particles, monomers, and bacterial cells to derive testable relationships of SOM kinetic parameters, including (1) maximum reaction rates and (2) binding half saturation constants (also known as substrate affinity parameters). We integrate the relevant mechanisms with the Equilibrium Chemistry Approximation (ECA) kinetics, which has been shown to reasonably represent these complex competitive interactions in soils, and then evaluate the reverse and forward Michaelis-Menten kinetics approximations under different conditions. We found: (1) due to the size contrast between larger organic polymer particles and smaller enzyme molecules, depolymerization is limited by the abundance of enzyme binding sites supplied by polymer particles, making the reverse Michaelis-Menten kinetics a better approximation to the ECA kinetics for depolymerization, and (2) due to the size contrast between larger microbial cells and smaller monomer molecules, monomer uptake is limited by accessible microbial cell transporters, making the forward Michaelis-Menten kinetics a better approximation to ECA kinetics for microbial monomer substrate uptake. These results may explain conflicting applications in the literature associated with using reverse and forward Michaelis-Menten kinetics to represent SOM dynamics. Further, the size contrast between litter particles and extracellular enzymes suggests that litter fragmentation by soil fauna and fungi is an important process to be included in models of organic matter decomposition and challenges soil enzyme assays to accurately measure enzyme abundances in order to properly derive the kinetic parameters.

1. Introduction

To make credible projections of the terrestrial carbon cycle and its interactions with climate, scientists modeling soil organic matter decomposition have called for more mechanistic representations of microbial dynamics (Wieder et al., 2015; Riley et al., 2020; Sulman et al., 2018). Such an approach would require better representations of internal microbial physiology (i.e., how microbes balance the trade-off between exoenzyme production with new growth), and more robust kinetic formulations of the external relationships between enzymes, microbes, abiotic processes (e.g., mineral surface interactions), and monomeric and polymeric substrates (i.e., how reacting agents interact with each other). For the latter, which is the focus here, a number of approaches have been proposed, including the classic forward Michaelis-Menten (fMM) or Monod type kinetics (Johnson and Goody, 2011; Michaelis and Menten, 1913; Monod, 1949), the reverse Michaelis-Menten (rMM) kinetics (Bailey, 1989; Schimel and Weintraub, 2003), the Equilibrium Chemistry Approximation (ECA) kinetics (Huang et al., 2018; Riley et al., 2018; Tang and Riley, 2013, 2015, 2017; Tang, 2015; Wang and Allison, 2019; Zhu et al., 2016, 2017), and the less frequently used Synthesizing Unit kinetics (Brandt et al., 2004; Kooijman, 1998, 2010). However, all these mathematical formulations (except ECA) were originally proposed for biogeochemical reactions in an aqueous environment. Therefore, even though it has rarely been discussed, whether these mathematical tools can be applied to soil biogeochemistry, which involves interactions between solid, gaseous, and aqueous phase entities, remains uncertain (e.g., see one reviewer's comment on Tang (2015)).

03

fMM kinetics represents biogeochemical reaction rates with a hyperbolic response to substrate availability and a linear dependence on the concentration of enzymes or agents that carry out the reaction. In contrast, rMM kinetics places the linear dependence on the substrate

mingxi zhang

* Corresponding author.
E-mail address: jinyuntang@lbl.gov (J. Tang).

https://doi.org/10.1016/j.soilbio.2019.107624
Received 14 June 2019; Received in revised form 4 October 2019; Accepted 6 October 2019
Available online 10 October 2019
0038-0717/

4-5
2 notes

concentration and a hyperbolic dependence on the enzyme concentration. Both of these approaches have solid experimental foundations (e.g., Michaelis and Menten, 1913; Kari et al., 2017) and successful modeling applications (e.g., Averill, 2014; Riley et al., 2014; S... al., 2018; Wang et al., 2013). However, Tang (2015) showed that fMM and rMM kinetics are two end members of the ECA kinetics, with fMM kinetics implicitly assuming that substrate is unlimiting while rMM kinetics assuming that enzyme is unlimiting. In soil, substrate availability is spatially and temporally variable, to which enzymes and consumers continuously respond (e.g., Hobbie and Hobbie, 2013). Therefore, neither fMM nor rMM kinetics is appropriate for the whole range of soil biogeochemical dynamics, a gap the ECA kinetics was designed to fill.

06

mingxi zhang

However, Moorhead and Weintraub (2018) recently argued that ECA kinetics has intrinsic difficulty in parameterizing the maximum consumption rate and affinity parameter of the enzyme-substrate complex, and recommended selecting between fMM and rMM kinetics based on the ratios of (1) enzyme to substrate concentrations and (2) maximum fMM and rMM reaction rates. Meanwhile, in studying enzymatic cellulose degradation, Kari et al. (2017) suggest that the kinetic parameters of fMM and rMM kinetics are related through the relationship between binding site and solid cellulose mass concentrations. Partially based on the argument by Kari et al., Andersen et al. (2018) contended that ECA kinetics (as well as the quadratic kinetics) can be applied to solid substrates. Moreover, Wang and Allison (2019) recently showed that ECA kinetics is able to effectively upscale the multiple-substrate-multiple-enzyme cellulose degradation simulated by a spatially-explicit and trait-based individual based model.

Soil biogeochemistry is a very complex and dynamic system, involving entities that range from monomeric molecules as small as nanometers to organic particles as large as centimeters, all of which are under the influence of transport over spatial scales of meters or longer. Therefore, estimating even the order of magnitudes of relevant kinetic parameters at a representative spatial scale (e.g., 1 cm in length) remains difficult. We show here that, for an enzyme-aided reaction, combining diffusion of the mobile entity and size of the immobile entity (and a few other measurable parameters that are often reported in the literature) enables a mechanistic explanation and reasonable estimation of the effective kinetic parameters, which therefore allows the application of ECA kinetics. We further show that both rMM and fMM kinetics are special approximations to the ECA kinetics, and rMM kinetics arises naturally for enzymatic depolymerization when no other enzyme binding surfaces (e.g., mineral soils) are present, whereas fMM kinetics emerges naturally for microbial uptake of monomeric substrates when

07

mingxi zhang

significant competitors (e.g., soil minerals) are present. Finally, because ECA kinetics allows a natural "process scaling" between these idealized conditions (Tang and Riley, 2013, 2017; Wang and Allison, 2019), we contend that it provides a potential path to improving soil biogeochemical formulations.

2. Conceptual framework

2.1. General concept

Our conceptual framework is based on the idea of a dissolved molecule interacting with a water-immersed solid particle through diffusion-aided binding, which forms a complex between the two that may or may not produce new molecules (Fig. 1). We consider two sets of interactions of this type. First, for enzymatic depolymerization, the enzyme is the dissolved molecule, and the polymeric organic aggregate is the solid particle (Fig. 1a). Second, for microbial uptake of monomeric substrates, the monomer is the dissolved molecule, and the microbial cell is the solid particle (Fig. 1b). A third set of interactions that describe monomer adsorption to soil minerals (e.g., monomer adsorption to clay particles, with the monomer being the dissolved molecule and the clay particle being the solid particle) can be similarly formulated with our conceptual framework (e.g., using information from Brusseau and Rao (1989) or Langmuir (1997)), but we will leave its discussion for future work.

Our conceptual framework can be traced back to the 100-year old classic model by Smoluchowski (1917) on how to compute diffusion-limited chemical reaction rates. The same conceptualization is also central to the Langmuir isotherm (Langmuir, 1918) and Hill's equation (Hill, 1910), where the former played an important role in the development of surface chemistry (Swenson and Stadie, 2019), and the latter in pharmacology (Goutelle et al., 2008). The Smoluchowski (1917) model has also been applied extensively to compute chemical reaction rates of various systems, including enzymatic reactions (Alberty and Hammes, 1958; Chou and Jiang, 1974). We recently exploited this conceptual framework to model how soil moisture regulates the effective affinity parameter describing microbial-substrate interactions, and found that it quite accurately reproduced soil moisture controls on heterotrophic soil respiration (Tang and Riley, 2019).

The pith of our conceptual framework can be summarized as follows (Fig. 1). For a large (about 1–100 μm in radius) solid particle immersed in water, a small (a few nanometers in radius) dissolved molecule can diffuse, intercept the solid particle surface, be captured at a binding site,

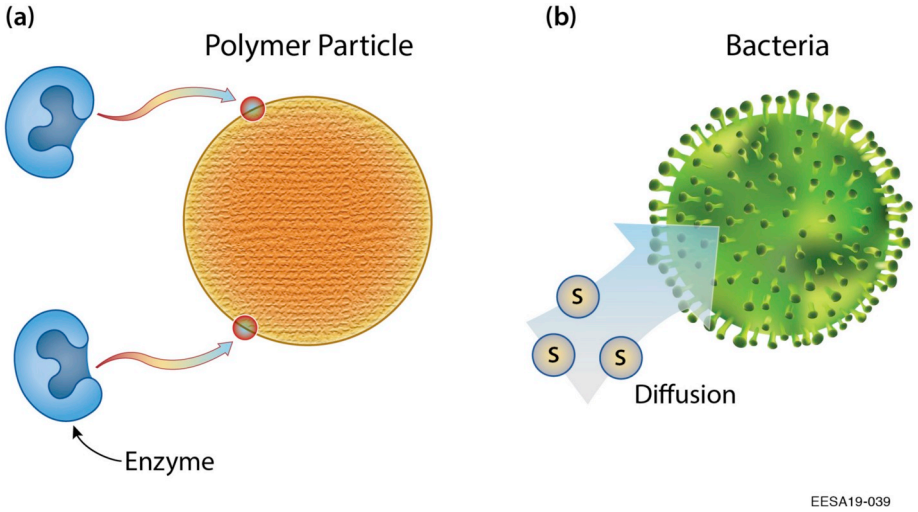

Fig. 1. Schematic of the diffusion-controlled binding of (a) enzymes (of radii R_E) to a polymer particle (of radius R_P), (b) dissolved substrate molecules (characterized by transporter radii r_p) to a bacteria cell (of radius r_c). In soil, $R_E \ll R_P$, i.e., the size of enzymes (~nm) is much smaller than that of the polymer particle (~μm); and $r_p \ll r_c$, i.e., the size of dissolved substrate (~nm) is much less than that of the bacteria cell (~μm).

and produce new molecules (if the binding is part of a chemical reaction). When the diffusion and post-binding processes (which could be either chemical conversion or desorption, or both) are in steady state, the overall system can be described, assuming equilibrium (Andersen et al., 2018; Briggs and Haldane, 1925; Tang and Riley, 2013), as:

$$k_1[S][P] = k_2[X] \quad (1)$$

where the concentration of a variable x is designated by $[x]$, so that with k_1, the coefficient of diffusion, $k_1[S]$ is the (normalized) diffusion flux of the dissolved molecule (whose concentration is $[S]$, assuming P as a perfect sink of S and the diffusion flux is normalized with respect to the binding sites (e.g., Berg and Purcell, 1977)), $[P]$ is the free binding sites per unit volume of water, and, with the coefficient of conversion k_2, $k_2[X]$ is the conversion flux of the complex X formed from the binding. Here and below, by following Tang and Riley (2017), we have assumed that the specific unbinding rate is much smaller than k_2. Such an assumption is usually valid at the population level for enzyme depolymerization (Nill et al., 2018) and microbial substrate uptake considering the long history of biological optimization of related enzymes (Albery and Knowles, 1976; Kooijman, 2010). Further, for all variables henceforth, we assume SI units unless stated otherwise.

Equation (1) can be rewritten as

$$[S][P] = K[X] \quad (2)$$

where $K\left(=\frac{k_2}{k_1}\right)$ is the dissociation parameter used in the Langmuir isotherm or affinity parameter used in fMM, rMM, and ECA kinetics (Tang, 2015); we henceforth call K the affinity parameter unless stated otherwise.

To apply the above conceptual framework, we must estimate the coefficient of diffusion k_1 and the coefficient of conversion k_2, which we describe below for enzymatic depolymerization and microbial uptake of a monomer substrate. Further, to simplify the problem, we consider only saturated conditions, which may or may not involve soil minerals and refer readers to Tang and Riley (2019) for methods to extend the results to variably saturated soils involving clusters of microbes. We note that confining the discussion to saturated conditions also allows our results to be applied to industrial lignocellulose degradation (e.g., Jeoh et al., 2017).

2.2. Enzymatic depolymerization

In formulating this problem, we assume all polymer particles are spherical with a mean radius R_P, acknowledging that this simplification may underestimate the binding surface area for non-spherical polymer particles of the same mass and density. In the soil (and similarly in aqueous environments), polymer particles may be produced from litter fragmentation by fauna, in combination with mechanical milling through various physical mechanisms (e.g., detritivore activity, soil shrinkage and expansion resulting from moisture and temperature changes, and so on; Burghouts et al., 1992; Graça, 2001; Petersen and Luxton, 1982; Vasconcelos and Laurance, 2005). In industrial bioreactors, polymer particles are produced from physical or chemical pretreatment combined with milling and sieving (Chundawat et al., 2008; Sangseethong et al., 1998). As for polymer particles, we assign extracellular enzymes a mean radius R_E. Assuming single-layer binding (as implied in the Langmuir isotherm), R_P and R_E can now be used to compute N_E the maximum number of enzyme molecules that can bind to a polymer particle, which we estimate as the ratio between enzyme attachable surface area of the polymer particle (i.e., a sphere of radius R_P with normalized binding density σ_{EP}) and the cross-section area of an enzyme molecule (i.e., a disc with radius R_E):

$$N_E = 4\sigma_{EP}\left(\frac{R_P}{R_E}\right)^2 \quad (3)$$

where σ_{EP} (unitless) is the fraction of allowed enzyme binding area over the polymer particle surface, which is determined by the enzyme chemical properties and the corresponding polymer. For cellulose, measurements suggest σ_{EP} is 0.1 for cellobiohydrolase I (Divne et al., 1998; Gao et al., 2013), whereas for other cases, we may simply assume that σ_{EP} equals one (in the absence of measurements). As mentioned above, in the assumptions that lead to the Langmuir isotherm, only one-layer enzyme adsorption to the polymer surface is considered in equation (3). Therefore, considering that polymer particle surfaces may be amorphous (which implies more surface area than that of a spherical particle of the same volume), N_E calculated by equation (3) is a lower bound to the kinetic surface as defined in Kari et al. (2017).

With equation (3) and V_E the maximum hydrolysis rate that each enzyme molecule is able to carry out, we compute the maximum polymer reaction rate per polymer particle (V_P) as

$$V_P = N_E V_E \quad (4)$$

For cellulose hydrolysis, V_E is a measurable parameter and varies insignificantly under room temperature and typical pH (5–6) conditions (e.g., Gao et al., 2013; Nill et al., 2018). Under natural conditions and for other enzymes, such as chitinase, V_E may vary significantly and new theories are needed for predictive applications (e.g., Ebrahimi et al., 2019a). However, such complications will not change our conclusions below.

Motivated by Andersen et al. (2018), we now assume that enzymes can only attack chemical bonds within a thickness R_E of the polymer particle. The potential maximum number of enzyme molecules per unit C mass of polymer can then be computed as

$$M_{PE} = \frac{N_E}{\chi_C N_A \rho_P 4\pi R_P^2 R_E} = \frac{\sigma_{EP}}{\pi \chi_C N_A \rho_P R_E^3} \quad (5)$$

where N_A is the Avogadro constant, χ_C is the fraction of polymer mass as carbon, ρ_P is the polymer mass density, and M_{PE} is of unit mol enzyme molecules per gram C polymer. From equation (5), M_{PE} is independent of polymer particle size, because we only account for the polymer mass involved in the enzyme attack. This approach assumes that enzymes peel monomers off the polymer particle layer by layer, while keeping the particle in some mean spherical shape (as in peeling an onion). We use the estimate from equation (5) to approximate the maximum adsorption capacity of the polymer particle, which is different from the kinetic surface sites computed from equation (3), and may be regarded as the upper bound of the available enzyme binding sites of given polymer particles; such a differentiation is also emphasized empirically in Kari et al. (2017).

Following Tang and Riley (2019), equations (3) and (4) are combined with the enzyme diffusion rate (i.e., take the ratio between V_P and the diffusion-based substrate flux normalized for a polymer particle) to compute the enzyme affinity with respect to the polymer binding site in an aqueous solution:

$$K_{EP,0} = \frac{V_P}{4\pi D_E R_P N_A}\left(\frac{N_E R_E}{N_E R_E + \pi R_P}\right)^{-1} = \frac{\sigma_{EP} R_P V_E}{\pi D_E R_E^2 N_A}\frac{4\sigma_{EP} R_P + \pi R_E}{4\sigma_{EP} R_P} \quad (6)$$

where the term $N_E R_E/(N_E R_E + \pi R_P)$ is the probability of intercepting enzyme molecules by the polymer particle (Berg and Purcell, 1977).

Under the quasi-steady-state approximation, i.e., the production and consumption of enzyme-substrate complexes are in rapid equilibrium (e.g., Andersen et al., 2018; Bond et al., 1998; Tang, 2015), the affinity parameter formulated in equation (6) defines the following equilibrium

$$[P][E] = K_{EP,0}[X_{EP}] \quad (7)$$

where $[P]$ is the effective number of free enzyme binding sites as provided by the polymer particles immersed in a unit volume of water, and $[E]$ is the free enzyme aqueous concentration. Accordingly, $[X_{EP}]$ represents the number of bound enzymes (or equivalently enzyme-bounded

sites) at the polymer surface. In application, we set $K_{EP,0}$ to the same units as $[E]$.

The equilibrium defined in equation (7) is subjected to two conservation constraints. First, the binding site conservation:

$$[P] + [X_{EP}] = [P]_T \tag{8}$$

where $[P]_T$ is the total binding sites (free $[P]$ plus bound $[X_{EP}]$) provided by the water immersed polymer particles. Second, the enzyme conservation relationship:

$$[E] + [X_{EP}] = [E]_T \tag{9}$$

where $[E]_T$ is the total enzyme concentration (free $[E]$ plus bound $[X_{EP}]$).

When equations (7)–(9) are solved to first order accuracy (Tang, 2015), we obtain the ECA formulation of enzyme-polymer complex

$$[X_{EP}] = \frac{[E]_T[P]_T}{K_{EP,0} + [E]_T + [P]_T} \tag{10}$$

By discarding the enzyme conservation relationship (i.e., assuming that enzyme is unlimited while substrate is limiting), we obtain the rMM formulation of enzyme-polymer complex:

$$[X_{EP}] = \frac{[E][P]_T}{K_{EP,0} + [E]} \tag{11}$$

Note equation (11) is formulated based on free enzyme concentration $[E]$.

Alternatively, by only considering the enzyme conservation relationship (i.e., assuming that enzyme is limiting while substrate is unlimited), we obtain the fMM formulation of enzyme-polymer complex:

$$[X_{EP}] = \frac{[E]_T[P]}{K_{EP,0} + [P]} \tag{12}$$

Note equation (12) uses the free binding site concentration $[P]$.

We will conduct some quantitative analyses of the above results in section 3.

2.3. Microbial uptake of monomers

For dissolved substrate (or monomer) uptake by microbes, Tang and Riley (2019) showed that the reference substrate affinity parameter can be formulated as

$$K_{SC,0} = \frac{V_S N_p}{4\pi D_S r_C N_A} \frac{N_p r_p + \pi r_C}{N_p r_p} \tag{13}$$

where N_p is the number of transporters (or carrier enzymes or pores) distributed over the microbial cell (e.g., Koch, 1995; Nikaido, 2003), V_S is the specific substrate uptake rate of the transporter, D_S is the aqueous substrate diffusivity, and r_p and r_c are radii of the transporter and microbial cell, respectively.

Under the quasi-steady-state approximation, equation (13) is related to the following equilibrium between the dissolved substrates and active microbes:

$$[B][S] = K_{SC,0}[X_{BS}] \tag{14}$$

where $[B]$ is the number of free transporters that are able to bind with the substrates $[S]$, and $[X_{BS}]$ is the substrate-bounded transporters.

Similar to the binding equilibrium between enzyme and polymer, the equilibrium described by equation (14) is also subjected to two constraints. First, the transporter conservation relationship

$$[B] + [X_{BS}] = [B]_T \tag{15}$$

Second, the substrate conservation:

$$[S] + [X_{BS}] = [S]_T \tag{16}$$

By solving equations (14)–(16) to first order accuracy, we obtain the ECA formulation:

$$[X_{BS}] = \frac{[S]_T[B]_T}{K_{SC,0} + [S]_T + [B]_T} \tag{17}$$

Following the traditional derivation of fMM kinetics (Johnson and Goody, 2011), we assume that enzyme is limiting while substrate is unlimited. Equations (14) and (15) lead to the fMM formulation of substrate-enzyme complex:

$$[X_{BS}] = \frac{[S][B]_T}{K_{SC,0} + [S]} \tag{18}$$

Note equation (18) is based on free substrate concentration $[S]$.

Because in the following section we will show that rMM kinetics is not very useful for estimating microbial uptake of monomers, the rMM formulation of $[X_{BS}]$ is not presented here.

3. Example quantitative applications

Below we present two example applications: (1) cellulose depolymerization as a representative of enzymatic depolymerization, and (2) microbial uptake of monomeric carbon as a representative of microbial uptake of dissolved substrates. With literature-derived empirical measurements, we compared our theory predictions with empirically measured affinity parameters and quantitative relationships between kinetic parameters and geometric sizes.

3.1. Cellulose degradation

In this application, we apply the results derived in section 2.2 to enzymatic hydrolysis of cellulose, for which many studies have analyzed how particle size affects the hydrolysis rate and provided sufficient data for applying and testing our theory. For example, Sangseethong et al. (1998) measured the maximum amount of enzyme adsorbed onto three size classes of microcrystalline cellulose (mean radii are 10 μm, 25 μm, and 50 μm). With the measured cellulose mass density (1.35 g cm^{-3}) and enzyme (i.e., *T. reesei* cellulases) molecular weight 48,000 g mol^{-1} and radius 3.29 nm, they found that the maximum mass of enzyme adsorbed were 55, 56, and 54 mg enzyme per g cellulose for the three size classes, respectively (which are essentially independent of substrate particle size). Using these numerical values for substrate and enzyme characteristics, we obtain from equation (5) the maximum amount of enzyme adsorbed as 53 mg enzyme per g cellulose, which is very close to the measured values. Further, this value is equivalent to 1.10 μmol enzyme per g cellulose, which is of the same order as values for cellulose I and III reported in Gao et al. (2013) (0.65–2.64 μmol enzyme per g cellulose). Unfortunately, Gao et al. did not report the sizes or molecular weights of their enzymes derived from *Trichoderma reesei* nor the mass density of their cellulose substrate. Considering 20% variation of the enzyme radius (likely a reasonable upper bound according to the protein data bank (https://www.rcsb.org)), equation (5) leads to values in agreement with the range reported by Gao et al. (2013).

3.1.1. Affinity parameter

We next compute the affinity parameters of enzyme adsorption to cellulose particles (and present the data-model comparison in Fig. 2). Since the cellulose particle radius is about 10^3 times the enzyme radius, the interception probability in equation (6) is approximately one, giving:

$$K_{EP,0} = \frac{\sigma_{EP} R_P V_E}{\pi D_E R_E^2 N_A} \tag{19}$$

indicating that for given mean enzyme characteristics, the affinity parameter increases as substrate particle size increases. Using: (1) the enzyme characteristics described in the previous paragraph (and in Table 1); (2) a typical maximum hydrolysis rate of 5 s^{-1} (Gao et al.,

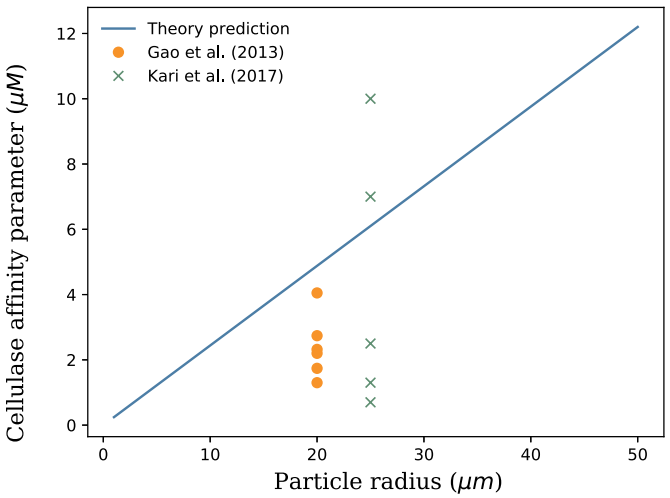

Fig. 2. Theory predicted cellulase affinity agrees well with experimental values from the literature. In this calculation, the cellulose particle radii are best guesses based on information provided in Gao et al. (2013) and Kari et al. (2017). The affinity parameters for Kari et al. (2017) were mean values estimated visually from their Figure 4D, ignoring their lower and upper bounds, which are about 0.3 μM and 12 μM, respectively.

2013; Nill et al., 2018) for cellulases derived from *T. reesei*; and (3) a typical enzyme diffusivity of 10^{-10} m^2 s^{-1} (if necessary, diffusivity of any enzyme molecule of known mass in solution can be estimated using the Stokes-Einstein equation (Miller, 1924) and the size-mass relationship (Erickson, 2009)), equation (19) leads to

$$K_{EP,0} = \frac{(0.1)(5s^{-1})R_P}{(3.142\cdot10^{-10}\mathrm{m^2 s^{-1}})(3.29\ \mathrm{nm})^2(6.02\cdot10^{23})} = 0.244\ \mathrm{M\ m^{-1}}R_P \quad (20)$$

Here and below "·" signifies multiplication.

Gao et al. (2013) reported affinity values ranging from 1.30 to 4.05 μM. However, they did not provide any information on the size distribution of their cellulose particles, so we assumed a median cellulose particle radius of 20 μm (from Chundawat et al. (2008), who used the same technique as Gao et al. (2013) for cellulose preparation), and with equation (20) we obtain $K_{EP,0}$ = 4.9 μM, which is slightly higher but of the same order of magnitude as their measured values (Fig. 2). Of four different types of cellulose degrading enzymes analyzed in Kari et al. (2017), their derived affinity parameters varied from 0.3 to 12 μM for cellulose Avicel PH101. Using the median radius of 25 μm reported from Sigma Aldrich's product description of Avicel PH101, equation (20) results in 6.1 μM, which is centered within the range of measured values (Fig. 2).

From equation (20), we see that the enzyme affinity parameter $K_{EP,0}$ is a linear function of particle radius (Fig. 2). This relationship is observed qualitatively in a study by Yeh et al. (2010), although they analyzed their results based on the fMM formulation (i.e., equation (12)) with substrate reported in polymer mass unit. Given the conversion coefficient α_{kin} (mol sites (kg substrate)$^{-1}$) between the kinetic binding sites and substrate mass:

$$\alpha_{kin} = \frac{(3)(4\sigma_{EP})}{4\rho\pi R_P^3 N_A}\left(\frac{R_P}{R_E}\right)^2 = \frac{3\sigma_{EP}}{\rho\pi R_P R_E^2 N_A} \quad (21)$$

the affinity parameter in polymer mass unit is:

$$K_{SP,kin} = \frac{\sigma_{EP}R_P V_E}{\pi D_E R_E^2 N_A}\alpha_{kin}^{-1} = \left(\frac{V_E}{3D_E}\right)\rho_P R_P^2 \quad (22)$$

Equation (22) shows that the affinity parameter in fMM kinetics decreases quadratically as the particle radius decreases rather than linearly as inferred in Yeh et al. (2010). We note that Yeh et al. (2010) used quite high enzyme concentrations (20 mg cellulase for 100 mL solution, or about 4167 μM assuming a mean enzyme molecular weight of 48K Da, and we were not able to extract their data to compute the parameters using the rMM kinetics), which were about 1000 times those used in Johnston et al. (1998), who also estimated the affinity parameter of fMM kinetics but with much lower enzyme concentrations. Nonetheless, by assuming a particle radius of 1 μm, the parameters used above lead to an affinity parameter computed from equation (22) of 22 g cellulose L^{-1}. This value is almost two orders of magnitude higher than that reported in Johnston et al. (1998), who reported values ranging from 0.334 to 1.307 g cellulose L^{-1} for four types of cellulases (but the V_E computed based on their Table 2 is about 0.5 s^{-1}, which if entered into equation (22) would correct our prediction to 2.2 g cellulose L^{-1}, slightly larger than their measurement-derived values). However, the 22 g cellulose L^{-1} value is within the range reported in Steiner et al. (1988), whose values range from 5 to 60 g cellulose L^{-1} using Avicel as substrate and *Trichoderma reesei* MCG 77 cellulase as the enzyme.

Interestingly, however, when the mass-based maximum sorption capacity (which can be derived from equation (5), and represents the upper bound of binding sites of a polymer particle) is used as the conversion coefficient, the following formula of affinity parameter (in polymer mass unit) is obtained

$$K_{SP,sorb} = \frac{\sigma_{EP}R_P V_E}{\pi D_E R_E^2 N_A}\left(\frac{\sigma_{EP}}{\pi N_A \rho_P R_E^3}\right)^{-1} = \left(\frac{V_E}{D_E}\right)R_E\rho_P R_P \quad (23)$$

which predicts a linear decrease of affinity parameter with decreasing cellulose particle size. Moreover, with the enzyme and substrate parameters used above, equation (23) predicts an affinity parameter of 0.22 mg mL^{-1} for substrate particles of a mean radius 1 μ*m*, which is about the same magnitude as reported in Johnston et al. (1998), whose description of substrate preparation implies that their particle size is a few μ*m*. This better agreement with measurements from equation (23) suggests another explanation for the above data-prediction discrepancy of fMM kinetics-based affinity parameter represented in mass units, i.e., in these experiments, the conversion coefficient between binding sites and substrate mass might be closer to the sorption capacity, probably because the enzymes were adsorbed both at the surface and intra-pores of cellulose particles, which resulted in a more complete correspondence between enzyme molecules and attackable sites. Finally, we note that these sorption experiments were usually longer than the burst hydrolysis period (about 30 min) that occurs upon the mixing of enzymes and cellulose (Nill et al., 2018). Therefore, during the data collection period of these experiments, cellulose was steadily hydrolyzed (Steiner et al., 1988), opening up more pore spaces in the polymer particles for enzyme adsorption. This dynamic hydrolysis brings the effective radius in equation (22) closer to $\sqrt{3R_E R_P}$, leading to lower sorption affinity parameters (denoted as $K_{SP,sorb}$) than the kinetic affinity parameters ($K_{SP,kin}$). Following the recommendation from Kari et al. (2017), we recommend using $K_{SP,kin}$ (and α_{kin}) for kinetic analysis.

Table 1
Literature derived characteristics of enzyme and polymer substrate used in this study (Gao et al., 2013; Divne et al., 1998; Nill et al., 2018; Sangseethong et al., 1998).

Enzyme	T. reesei cellulases
Molecular weight	48,000 g mol^{-1}
Radius	3.29 nm
Specific hydrolysis rate V_E	5 s^{-1}
Diffusivity	10^{-10} s m^{-2}
Polymer substrate	Cellulose
Mass density ρ_P	1.35 g cm-3
Fraction of effective binding area σ_{EP}	0.1

3.1.2. Maximum depolymerization rate

We below make some qualitative assertions on how depolymeriza-

tion rate will change with cellulose particle size. Beginning with equation (11), the hydrolysis rate can be calculated as:

$$\frac{d[P]_T}{dt} = -V_E[X_{EP}] = -\frac{V_E[E][P]_T}{K_{EP,0}+[E]} \quad (24)$$

where $[P]_T$ (mol sites m^{-3}) is the water immersed polymer substrate concentration, and $[E]$ (mol enzymes m^{-3}) is the exoenzyme concentration. Therefore, when equation (24) is written for the total carbon mass of polymer particles in the size class of radius R_P, the hydrolysis rate is

$$\frac{d[M_{RP}]}{dt} = -\left(\frac{12[M_{RP}]}{\chi_C N_A 4\pi R_P^3 \rho_R/3}\right)\cdot(12V_P)\cdot\left(\frac{[E]}{K_{EP,0}+[E]}\right) \quad (25)$$

where $[M_{RP}]$ (mol C m^{-3}) is the concentration of water immersed polymer particles, the first right-hand side (RHS) term is the total number of polymer particles (mol m^{-3}) with 12 being the molar weight of carbon. The number 12 in the second RHS term is the number of carbon atoms per cellobiose molecule (the main product of processive cellulose hydrolysis (e.g., Nill et al., 2018)). Combining equation (25) with the definition of V_P from equation (4), we obtain the maximum hydrolysis rate ($k_{max,RP}$; s^{-1}) for size class of radius R_P:

$$k_{max,RP} = \frac{(144)(4V_E\sigma_{EP})(R_P/R_E)^2}{\chi_C N_A 4\pi R_P^3\rho_R/3} = \frac{432V_E\sigma_{EP}}{\chi_C N_A \pi R_P R_E^2 \rho_R} \quad (26)$$

Using the carbon mass content of cellulose (0.44) and the typical numerical values of enzyme and substrate characteristics described above, we have

$$k_{max,RP} \approx 1.8\times10^{-11}R_P^{-1} \quad (27)$$

which suggests that the larger the particle size, the slower the maximum hydrolysis rate, as observed in Yeh et al. (2010). Further, because our derivation above is generic, this inverse proportionality should be applicable to organic particles in general, albeit with different numeric values of the slope due to the variability of V_E under different conditions for different enzymes (e.g., Ebrahimi et al., 2019a) and other geometric shapes.

With equation (26), we then have

$$\frac{d[M_{RP}]}{dt} = -k_{max,RP}[M_{RP}]\frac{[E]}{K_{EP,0}+[E]} \quad (28)$$

from which (by noticing $[M_{RP}]\propto R_P^3$) we can derive the temporal evolution of particle radius as

$$\frac{dR_P}{dt} = -\frac{R_P}{3}\frac{k_{max,RP}[E]}{K_{EP,0}+[E]} \quad (29)$$

However, we note that equations (25), (28) and (29) do not consider the product inhibition effect (Yeh et al., 2010).

3.2. Microbial uptake of monomers

Our calculation below is based on typical characteristics of bacterial cells, and ignores complications associated with, e.g., variability in the number of transporters per cell and V_S due to different microbial physiological status. Future research should work to develop the theoretical structure to account for these effects and relevant observations for model parameterization. However, including such complications is unlikely to affect the basic relationships we describe here. Analysis of fungi is left to future studies. We begin with the assumption of a typical bacterial cell of radius 1 μm. To compute the number of transporters per unit carbon microbial biomass, we use an allometric relationship for moles of microbial cells per mol C biomass (λ_B). Based on data from Loferer-Krossbacher et al. (1998), Tang and Riley (2019) obtained a value $\lambda_B = 2.68\times10^{-11}$ mol cells (mol C)$^{-1}$, while the data from Bratbak and Dundas (1984) lead to a value $\lambda_B = 2.1\times10^{-11}$ mol cells (mol C)$^{-1}$. With λ_B the total number of transporters per g carbon biomass of microbes is:

$$N_{SB} = \lambda_B N_P/12 \quad (30)$$

Following Tang and Riley (2019), we here adopt a 50% probability of intercepting monomer molecules, which leads to $N_P = 3140$ transporters per cell (covering 0.08% cell surface), and $N_{SB} = 5.5\times10^{-9}$ mol transporters (g C biomass)$^{-1}$.

For a typical monomer substrate (e.g., small molecular weight sugar) diffusivity of 5×10^{-10} m^2 s^{-1} (Cussler, 1984) and a transporter maximum specific substrate uptake processing rate $V_S = 100\ s^{-1}$ (Koch, 1995; Milo and Phillips, 2015), with equation (13) we obtain the substrate affinity $K_{SC,0}$ as 1.6×10^{-4} mol molecule m^{-3} or 1.6×10^{-1} μM molecules, within the range of measured values (e.g., Button, 1985). Accordingly, the maximum substrate uptake rate is 5.5×10^{-7} mol substrate (g C biomass)$^{-1}$ s^{-1}, which for a carbon substrate with 10 carbon atoms is 5.5×10^{-6} mol C (g C biomass)$^{-1}$ s^{-1} or 6.6×10^{-5} g C (g C biomass)$^{-1}$ s^{-1}. This last value is of the same order of magnitude as obtained through calibration in several existing soil biogeochemical models (e.g., Dwivedi et al., 2017 (2.8×10^{-6} g C (g C biomass)$^{-1}$ s^{-1}); Grant, 2013 (3.4×10^{-5}g C (g C biomass)$^{-1}$ s^{-1}); Maggi et al., 2008 (4.49×10^{-6} g C (g C biomass)$^{-1}$ s^{-1})) and agrees with that has been inferred from measurements (e.g., Shields et al. (1973), which was used in Grant (2013)).

4. Discussion

4.1. Which kinetic formulation to use: fMM, rMM, or ECA?

We now discuss the kinetic formulations of two processes that are relevant to soil biogeochemical modeling.

4.1.1. Depolymerization

We start our analysis with the ECA formulation of cellulose degradation

$$\frac{d[P_M]_T}{dt} = -\chi_0\frac{V_E[E]_T\alpha_{kin}[P_M]_T}{K_{EP,0}+[E]_T+\alpha_{kin}[P_M]_T} \quad (31)$$

where $[P_M]_T$ (mol C m^{-3}) is the water immersed solid cellulose concentration, which can be converted into binding sites (mol sites m^{-3}) via α_{kin}, $[E]_T$ (mol m^{-3}) is the total concentration of cellulases (free plus bound), and χ_0 is the number of carbon atoms per product molecule.

Given typical enzyme characteristics (Table 1), 1 g cellulose with a particle radius of 1 μm has total available binding sites ($\alpha_{kin}[P_M]_T$) of 1.1×10^{-8}mol. When this cellulose is added to 100 mL solution, the binding site concentration is 1.1×10^{-7}mol L^{-1}. Also, 20 mg cellulase (in 100 mL) is about 4.2×10^{-7} mol, or 4.2 μM. Therefore, considering that the highest substrate amount used by Yeh et al. (2010) is 0.1 g cellulose per 100 mL solution, the ratio between effective enzyme binding sites and enzyme abundance is smaller than 1% (i.e., 1.1/420), suggesting that their system can be reasonably approximated with the rMM kinetics (i.e., removing $\alpha_{kin}[P_M]_T$ from the denominator of equation (31)). Further, for larger cellulose particles, α_{kin} becomes smaller (as can be inferred from equation (21)), so that $\alpha_{kin}[P_M]_T$ will decrease further, making the system even more substrate limited, and the approximation by rMM kinetics even more accurate. Using Avicel PH101 as substrate, Kari et al. (2017) experimented with cellulose loading as high as 80 g L^{-1}, which under the assumption of 1 μm particle radius, resulted in a substrate to enzyme binding sites ratio of 0.21 (i.e., 88/420). However, particle radius of Avicel PH101 often varies between 5.0 μm and 30.0 μm (e.g., Levis and Deasy, 2001), the linear reduction of α_{kin} with increasing radius (as can be inferred from equation (21)) will drive the ratio of substrate to enzyme binding sites to be smaller than 5%, and, once

again, the system is in the validity domain of rMM kinetics (an assertion that is also made by Kari et al. (2017) based on their data).

Next, we analyze the scenario in soil. Given 20 mg cellulase per 1 g cellulose (of radius 1 μm), the mass ratio of the system is 1/50 (2%), and the mole ratio between binding sites and enzymes is 1.1/420 (0.26%). Soil microbial biomass is usually no more than 10% of the total soil carbon stock (e.g., Ladd et al., 1994). By assuming that extracellular enzymes are as much as half of the total microbial biomass (which is very likely an overestimate as can be inferred from empirical experiments (e.g., Rinkes et al., 2013), but gives a mass ratio comparable to the example used here), the resultant mole ratio of enzyme binding sites to extracellular enzyme amount is therefore only a few percent. Soil organic matter, particularly where unprocessed plant material dominates, may very likely have large particle radii (e.g., larger than 1 mm), and (as implied in the formulation of α_{kin}) larger particle sizes will proportionally reduce the mole ratio between binding sites and enzymes. Therefore, soil organic matter depolymerization is very likely substrate (i.e., binding sites) limited (and this assertion is independent from the biogeochemical variability of catalysis rate V_E or enzyme type), and would be better described by the rMM kinetics or ECA kinetics. There is one exception though: for inoculation experiments, where enzyme concentrations are small compared to substrates, the initial period may better be approximated by fMM and ECA kinetics.

For pure polymeric substrates, the inferred particle size dependence of kinetic parameters in section 3.1 should be generally correct. Different geometric shapes or porosity structure are expected to only change the magnitude of such dependence, but the trend that larger polymer particles will be degraded slower will remain. For natural organic matter that includes multiple chemical structures, e.g. plant material that contains carbohydrate, lipid, cellulose and lignin concurrently, the size dependence for the hydrolysis of each chemical component may be more complicated. However, our previous success in partly explaining the lignin-induced slowdown of litter decomposition using the ECA kinetics (Tang and Riley, 2013) encourages us to hypothesize that combining the separately computed kinetics parameters (as done for cellulose here) in an ECA representation of the multi-substrate-multi-consumer network may produce predictions largely consistent with existing measurements. Such an analysis should be the focus of future work.

4.1.2. Monomer uptake

Following equation (17), the ECA formulation of monomer uptake is:

$$\frac{d[S]_T}{dt} = -V_S \frac{[S]_T N_{SB}[B_M]}{K_{SC,0} + [S]_T + N_{SB}[B_M]} \quad (32)$$

where $[B_M]$ (g C m^{-3}) is microbial biomass, which is converted into binding sites with N_{SB}. As in the depolymerization case, the ratio of substrate $[S]_T$ to transporter concentration $N_{SB}[B_M]$ determines whether fMM or rMM kinetics better approximates the ECA kinetics. Previously, we showed that N_{SB} is about 5.5×10^{-9} mol transporters (g C biomass)$^{-1}$. With a mean monomer carbon content of about 10 carbon atoms per molecule, the mole ratio of dissolved organic carbon (DOC) to moles of transporter for 1 g C DOC vs 1 g C of biomass is approximately $1 \div 120 \div (5.5 \times 10^{-9}) = 1.5 \times 10^{6}$. Therefore, unless DOC is above about 1 ppm of microbial cell biomass, an unlikely low value in soil, the amount of monomer substrates exceeds that of bacterial transporters (and microbial physiology is unlikely to change this contrast), suggesting that, in the absence of other DOC sorbents, microbial DOC uptake better follows fMM or ECA kinetics.

4.2. Implications to soil organic matter decomposition modeling

4.2.1. Importance of litter fragmentation

Our analyses above demonstrate that the larger the polymer particles are, the slower they will be depolymerized. This assertion is well corroborated by experimental studies of enzymatic cellulose degradation (Yeh et al., 2010). Both our calculations and the empirical experiments in Yeh et al. (2010) show that smaller particle size influences enzymatic depolymerization rate by increasing the maximum depolymerization rate and reducing the substrate affinity parameter (so that enzyme-polymer binding is more favored). This relationship suggests that for the same amount of litter carbon mass, litter particles of 1 mm radius will be depolymerized about 10^3 times slower than those of radius 1 μm. In most ecosystems, new litter particles often have radii much larger than 1 mm, with wood having radii orders of magnitude larger than that (Kirk and Cowling, 1984). Therefore, free-living microorganisms must develop ways to overcome the barrier imposed on extracellular enzyme diffusion and their small binding opportunities to substrates during depolymerization. In nature, one such way is to become multicellular, either functionally or biologically, such as microbes aggregating together to share public goods and reduce the leakage of hydrolysis products (e.g., Ebrahimi et al., 2019b; Julou et al., 2013). Litter fragmentation by soil fauna or penetrative fungi hyphae, a corollary well supported by existing empirical studies (e.g., King et al., 2018; van der Wal et al., 2007), showing that removing detritivores often slows down litter fragmentation and reduces litter decomposition (Burghouts et al., 1992; Graça, 2001; Petersen and Luxton, 1982). Therefore, to mechanistically resolve the biogeochemical dynamics of litter and soil organic matter, models would benefit from explicitly considering fragmentation (as was done in some early models, e.g., Smith, 1979) by representing trophic relationships between litter, decomposers and detritivores (e.g., Hunt et al., 1987). For the latter, the ECA kinetics in its multi-consumer-multi-substrate form will be an effective approach at scaling these complex interactions (Tang and Riley, 2013; Riley et al., 2020; Wang and Allison, 2019).

4.2.2. Importance of abiotic sorption surfaces

From Mayes et al. (2012), the typical DOC Langmuir affinity is about (1–100 mg L^{-1}), and sorption capacity is about 0.100–5 mg (g soil)$^{-1}$, whereas typical soil organic carbon content is about 10 mg (g soil)$^{-1}$. Therefore, the DOC binding sites from soil sorbent is often much higher than that of bacterial cells and may act as important competitive inhibitors of microbial uptake of organic monomers. Similarly, because the sizes of enzyme molecules and DOC are both about a few nanometers, abiotic sorption surfaces are important in modifying enzymatic depolymerization (e.g., Allison, 2006; Quiquampoix and Burns, 2007). Both of these processes fall neatly within the application domain of the ECA kinetics, which was used in the Reaction-network-based model of Soil Organic Matter and Microbes (ReSOM) model that was able to realistically simulate many features of soil carbon dynamics (Tang and Riley, 2015; Abramoff et al., 2019) and in the nutrient competition model to simulate plant-microbial interactions (Zhu et al., 2016, 2017).

5. Conclusion

Based on diffusion theory and the size contrast between enzymes and polymer particles during depolymerization, and that between microbes and monomer substrates during microbial uptake, we developed equations to estimate substrate affinity parameters and maximum substrate processing rates. With typical characteristics of extracellular enzymes, polymer particles, microbes, and monomeric organic carbon substrates, our framework was able to make a number of inferences that agree well with experiments and calibrated parameters from existing models. In particular, our results indicate that for enzymatic depolymerization, large polymer particles will be depolymerized slower due to binding site (per mass) limitation to enzymes, which in turn suggests that litter fragmentation is an important process to consider in studying soil organic matter formation and decomposition. Further, we showed that enzymatic depolymerization more closely follows the reverse Michaelis-Menten kinetics, while microbial uptake of soluble substrates more closely follows the forward Michaelis-Menten kinetics. Since many

current studies quantify enzyme kinetics using the forward Michaelis-Menten kinetics (e.g., Allison, 2006; Loeppmann et al., 2016), our results suggest improved methods for experimentalists to analyze their data. In particular, it raises a serious challenge to accurately quantify the often difficult-to-measure soil enzyme concentrations and diversity. Finally, because soil biogeochemistry is a complex network of multiple phases, substrates, and competitors, the Equilibrium Chemistry Approximation kinetics, which spans these end member cases, is likely an effective modeling framework for soil biogeochemistry.

Declaration of competing interest

The authors declare that they have no known competing financial interests or personal relationships that could have appeared to influence the work reported in this paper.

Acknowledgements

This research was supported by the Director, Office of Science, Office of Biological and Environmental Research of the US Department of Energy under contract no. DE-AC02-05CH11231 as part of the TES Soil Warming SFA and the Next Generation Ecosystem Experiment-Arctic project. Financial support does not constitute an endorsement by the Department of Energy of the views expressed in this study. Comments from the editor and two reviewers have significantly improved an earlier version of this manuscript.

Appendix A. Supplementary data

Supplementary data to this article can be found online at https://doi.org/10.1016/j.soilbio.2019.107624.

References

Abramoff, R.Z., Torn, M.S., Georgiou, K., Tang, J.Y., Riley, W.J., 2019. Soil organic matter temperature sensitivity cannot be directly inferred from spatial gradients. Global Biogeochemical Cycles 33, 761–776.
Albery, W.J., Knowles, J.R., 1976. Evolution of enzyme function and development of catalytic efficiency. Biochemistry 15, 5631–5640.
Alberty, R.A., Hammes, G.G., 1958. Application of the theory of diffusion-controlled reactions to enzyme kinetics. Journal of Physical Chemistry 62, 154–159.
Allison, S.D., 2006. Soil minerals and humic acids alter enzyme stability: implications for ecosystem processes. Biogeochemistry 81, 361–373.
Andersen, M., Kari, J., Borch, K., Westh, P., 2018. Michaelis-Menten equation for degradation of insoluble substrate. Mathematical Biosciences 296, 93–97.
Averill, C., 2014. Divergence in plant and microbial allocation strategies explains continental patterns in microbial allocation and biogeochemical fluxes. Ecology Letters 17, 1202–1210.
Bailey, C.J., 1989. Enzyme-kinetics of cellulose hydrolysis. Biochemical Journal 262, 1001-1001.
Berg, H.C., Purcell, E.M., 1977. Physics of chemoreception. Biophysical Journal 20, 193–219.
Bond, R.A.B., Martincigh, B.S., Mika, J.R., Simoyi, R.H., 1998. The quasi-steady-state approximation: numerical validation. Journal of Chemical Education 75, 1158–1165.
Brandt, B.W., Kelpin, F.D.L., van Leeuwen, I.M.M., Kooijman, S.A.L.M., 2004. Modelling microbial adaptation to changing availability of substrates. Water Research 38, 1003–1013.
Bratbak, G., Dundas, I., 1984. Bacterial dry-matter content and biomass estimations. Applied and Environmental Microbiology 48, 755–757.
Briggs, G.E., Haldane, J.B.S., 1925. A note on the kinetics of enzyme action. Biochemical Journal 19, 338–339.
Brusseau, M.L., Rao, P.S.C., 1989. The influence of sorbate-organic matter interactions on sorption nonequilibrium. Chemosphere 18, 1691–1706.
Burghouts, T., Ernsting, G., Korthals, G., Devries, T., 1992. Litterfall, leaf litter decomposition and litter invertebrates in primary and selectively logged dipterocarp forest in Sabah, Malaysia. Philosophical Transactions of the Royal Society of London Series B Biological Sciences 335, 407–416.
Button, D.K., 1985. Kinetics of nutrient-limited transport and microbial-growth. Microbiological Reviews 49, 270–297.
Chou, K.C., Jiang, S.P., 1974. Studies on the rate of diffusion-controlled reactions of enzymes. Spatial factor and force field factor. Scientia Sinica 27 (5), 664–680.
Chundawat, S.P.S., Balan, V., Dale, B.E., 2008. High-throughput microplate technique for enzymatic hydrolysis of lignocellulosic Biomass. Biotechnology and Bioengineering 99, 1281–1294.
Cussler, E.L., 1984. Diffusion: Mass Transfer in Fluid Systems. Cambridge University Press, Cambridge.
Dwivedi, D., Riley, W.J., Torn, M.S., Spycher, N., Maggi, F., Tang, J.Y., 2017. Mineral properties, microbes, transport, and plant-input profiles control vertical distribution and age of soil carbon stocks. Soil Biology and Biochemistry 107, 244–259.
Divne, C., Stahlberg, J., Teeri, T.T., Jones, T.A., 1998. High-resolution crystal structures reveal how a cellulose chain is bound in the 50-angstrom long tunnel of cellobiohydrolase I from Trichoderma reesei. Journal of Molecular Biology 275, 309–325.
Ebrahimi, A., Schwartzman, J., Cordero, O.X., 2019. Cooperation and Spatial Self-Organization Determine Ecosystem Function for Polysaccharide-Degrading Bacteria. https://doi.org/10.1101/640961 bioRxiv preprint.
Ebrahimi, A., Schwartzman, J., Cordero, O.X., 2019. Multicellular Behavior Enables Cooperation in Microbial Cell Aggregates. https://doi.org/10.1101/626481 bioRxiv preprint.
Erickson, H.P., 2009. Size and shape of protein molecules at the nanometer level determined by sedimentation, gel filtration, and electron microscopy. Biological Procedures Online 11, 32–51.
Gao, D.H., Chundawat, S.P.S., Sethi, A., Balan, V., Gnanakaran, S., Dale, B.E., 2013. Increased enzyme binding to substrate is not necessary for more efficient cellulose hydrolysis. Proceedings of the National Academy of Sciences of the United States of America 110, 10922–10927.
Goutelle, S., Maurin, M., Rougier, F., Barbaut, X., Bourguignon, L., Ducher, M., Maire, P., 2008. The Hill equation: a review of its capabilities in pharmacological modelling. Fundamental & Clinical Pharmacology 22, 633–648.
Graça, M.A.S., 2001. The role of invertebrates on leaf litter decomposition in streams - a review. International Review of Hydrobiology 86, 383–393.
Grant, R.F., 2013. Modelling changes in nitrogen cycling to sustain increases in forest productivity under elevated atmospheric CO_2 and contrasting site conditions. Biogeosciences 10, 7703–7721.
Hill, A.V., 1910. The combinations of haemoglobin with oxygen and with carbon monoxide. International Journal of Physics 40, iv–vii.
Hobbie, J.E., Hobbie, E.A., 2013. Microbes in nature are limited by carbon and energy: the starving-survival lifestyle in soil and consequences for estimating microbial rates. Frontiers in Microbiology 4.
Huang, Y., Guenet, B., Ciais, P., Janssens, I.A., Soong, J.L., Wang, Y.L., Goll, D., Blagodatskaya, E., Huang, Y.Y., 2018. ORCHIMIC (v1.0), a microbe-mediated model for soil organic matter decomposition. Geoscientific Model Development 11, 2111–2138.
Hunt, H.W., Coleman, D.C., Ingham, E.R., Ingham, R.E., Elliott, E.T., Moore, J.C., Rose, S. L., Reid, C.P.P., Morley, C.R., 1987. The detrital food web in a shortgrass prairie. Biology and Fertility of Soils 3, 57–68.
Jeoh, T., Cardona, M.J., Karuna, N., Mudinoor, A.R., Nill, J., 2017. Mechanistic kinetic models of enzymatic cellulose hydrolysisA review. Biotechnology and Bioengineering 114, 1369–1385.
Johnson, K.A., Goody, R.S., 2011. The original Michaelis constant: translation of the 1913 Michaelis-Menten paper. Biochemistry 50, 8264–8269.
Johnston, D.B., Shoemaker, S.P., Smith, G.M., Whitaker, J.R., 1998. Kinetic measurements of cellulase activity on insoluble substrates using disodium 2,2 ' bicinchoninate. Journal of Food Biochemistry 22, 301–319.
Julou, T., Mora, T., Guillon, L., Croquette, V., Schalk, I.J., Bensimon, D., Desprat, N., 2013. Cell-cell contacts confine public goods diffusion inside Pseudomonas aeruginosa clonal microcolonies. Proceedings of the National Academy of Sciences of the United States of America 110, 12577–12582.
Kari, J., Andersen, M., Borch, K., Westh, P., 2017. An inverse Michaelis-Menten approach for interfacial enzyme kinetics. ACS Catalysis 7, 4904–4914.
King, J.R., Warren II, R.J., Maynard, D.S., Bradford, M.A., 2018. Ants: ecology and impacts in dead wood. In: Ulyshen, M.D. (Ed.), Saproxylic Insects: Diversity, Ecology and Conservation. Springer, Heidelberg, pp. 237–262.
Kirk, T.K., Cowling, E.B., 1984. Biological decomposition of solid wood. Advances in Chemistry Series 207, 2515–2519.
Koch, A.L., 1995. Bacterial Growth and Form. Chapman and Hall, New York.
Kooijman, S.A.L.M., 1998. The Synthesizing Unit as model for the stoichiometric fusion and branching of metabolic fluxes. Biophysical Chemistry 73, 179–188.
Kooijman, S.A.L.M., 2010. Dynamic Energy Budget Theory for Metabolic Organisation. Cambridge University Press, Cambridge.
Ladd, J.N., Amato, M., Zhou, L.K., Schultz, J.E., 1994. Differential-effects of rotation, plant residue and nitrogen-fertilizer on microbial biomass and organic-matter in an Australian alfisol. Soil Biology and Biochemistry 26, 821–831.
Langmuir, I., 1918. The adsorption of gases on plane surfaces of glass, mica and platinum. Journal of the American Chemical Society 40, 1361–1403.
Langmuir, D., 1997. Aqueous Environmental Geochemistry. Prentice Hall, Upper Saddle River, NJ.
Levis, S.R., Deasy, P.B., 2001. Production and evaluation of size reduced grades of microcrystalline cellulose. International Journal of Pharmaceutics 213, 13–24.
Loferer-Krossbacher, M., Klima, J., Psenner, R., 1998. Determination of bacterial cell dry mass by transmission electron microscopy and densitometric image analysis. Applied and Environmental Microbiology 64, 688–694.
Loeppmann, S., Biagodatskaya, E., Pausch, J., Kuzyakov, Y., 2016. Enzyme properties down the soil profile - a matter of substrate quality in rhizosphere and detritusphere. Soil Biology and Biochemistry 103, 274–283.
Maggi, F., Gu, C., Riley, W.J., Hornberger, G.M., Venterea, R.T., Xu, T., Spycher, N., Steefel, C., Miller, N.L., Oldenburg, C.M., 2008. A mechanistic treatment of the dominant soil nitrogen cycling processes: model development, testing, and application. Journal of Geophysical Research-Biogeosciences 113.

Mayes, M.A., Heal, K.R., Brandt, C.C., Phillips, J.R., Jardine, P.M., 2012. Relation between soil order and sorption of dissolved organic carbon in temperate subsoils. Soil Science Society of America Journal 76, 1027–1037.
Michaelis, L., Menten, M.L., 1913. Die kinetik der invertinwirkung. Biochemische Zeitschrift 49, 333–369.
Miller, C.C., 1924. The Stokes Einstein law for diffusion in solution. Proceedings of the Royal Society of London - Series A: Containing Papers of a Mathematical and Physical Character 106, 724–749.
Milo, R., Phillips, R., 2015. Cell Biology by the Numbers. Garland Sci., New York.
Monod, J., 1949. The growth of bacterial cultures. Annual Review of Microbiology 3, 371–394.
Moorhead, D.L., Weintraub, M.N., 2018. The evolution and application of the reverse Michaelis-Menten equation. Soil Biology and Biochemistry 125, 261–262.
Nikaido, H., 2003. Molecular basis of bacterial outer membrane permeability revisited. Microbiology and Molecular Biology Reviews 67, 593–656.
Nill, J., Karuna, N., Jeoh, T., 2018. The impact of kinetic parameters on cellulose hydrolysis rates. Process Biochemistry 74, 108–117.
Petersen, H., Luxton, M., 1982. A comparative-analysis of soil fauna populations and their role in decomposition processes. Oikos 39, 287–388.
Quiquampoix, H., Burns, R.G., 2007. Interactions between proteins and soil mineral surfaces: Environmental and health consequences. Elements 3, 401–406.
Riley, W.J., Zhu, Q., Tang, J.Y., 2018. Weaker land-climate feedbacks from nutrient uptake during photosynthesis-inactive periods. Nature Climate Change 8, 1002–1006.
Riley, W.J., Sierra, C., Tang, J.Y., Bouskill, N.J., Zhu, Q., Abramoff, R., 2020. Next generation soil biogeochemistry model representations: a proposed community open source model farm (BeTR-S), accepted. In: Yang, Y., Keiluweit, M., Senesi, N., Xing, B. (Eds.), Multi-scale Biogeochemical Processes in Soil Ecosystems: Critical Reactions and Resilience to Climate Changes. John Wiley and Sons, Inc.
Rinkes, Z.L., Sinsabaugh, R.L., Moorhead, D.L., Grandy, A.S., Weintraub, M.N., 2013. Field and lab conditions alter microbial enzyme and biomass dynamics driving decomposition of the same leaf litter. Frontiers in Microbiology 4.
Sangseethong, K., Meunier-Goddik, L., Tantasucharit, U., Liaw, E.T., Penner, M.H., 1998. Rationale for particle size effect on rates of enzymatic saccharification of microcrystalline cellulose. Journal of Food Biochemistry 22, 321–330.
Schimel, J.P., Weintraub, M.N., 2003. The implications of exoenzyme activity on microbial carbon and nitrogen limitation in soil: a theoretical model. Soil Biology and Biochemistry 35, 549–563.
Shields, J.A., Paul, E.A., Lowe, W.E., 1973. Turnover of microbial tissue in soil under field conditions. Soil Biology and Biochemistry 5, 753–764.
Sihi, D., Davidson, E.A., Chen, M., Savage, K.E., Richardson, A.D., Keenan, T.F., Hollinger, D.Y., 2018. Merging a mechanistic enzymatic model of soil heterotrophic respiration into an ecosystem model in two AmeriFlux sites of northeastern USA. Agricultural and Forest Meteorology 252, 155–166.
Smith, O.L., 1979. An analytical model of the decomposition of soil organic matter. Soil Biology and Biochemistry 11, 585–606.
Smoluchowski, M.V., 1917. Versuch einer mathematischen theorie der koagulationskinetik kolloider losungen. Zeitschrift f. Physik. Chemie. XCII 92, 129–168.
Steiner, W., Sattler, W., Esterbauer, H., 1988. Adsorption of trichoderma-reesei cellulase on cellulose - experimental-data and their analysis by different equations. Biotechnology and Bioengineering 32, 853–865.
Sulman, B.N., Moore, J.A.M., Abramoff, R., Averill, C., Kivlin, S., Georgiou, K., Sridhar, B., Hartman, M.D., Wang, G.S., Wieder, W.R., Bradford, M.A., Luo, Y.Q., Mayes, M.A., Morrison, E., Riley, W.J., Salazar, A., Schimel, J.P., Tang, J.Y., Classen, A.T., 2018. Multiple models and experiments underscore large uncertainty in soil carbon dynamics. Biogeochemistry 141, 109–123.
Swenson, H., Stadie, N.P., 2019. Langmuir's theory of adsorption: a centennial review. Langmuir 35 (16), 5409–5426.
Tang, J.Y., Riley, W.J., 2013. A total quasi-steady-state formulation of substrate uptake kinetics in complex networks and an example application to microbial litter decomposition. Biogeosciences 10, 8329–8351.
Tang, J.Y., Riley, W.J., 2015. Weaker soil carbon-climate feedbacks resulting from microbial and abiotic interactions. Nature Climate Change 5, 56–60.
Tang, J.Y., 2015. On the relationships between the Michaelis-Menten kinetics, reverse Michaelis-Menten kinetics, equilibrium chemistry approximation kinetics, and quadratic kinetics. Geoscientific Model Development 8, 3823–3835.
Tang, J.Y., Riley, W.J., 2017. SUPECA kinetics for scaling redox reactions in networks of mixed substrates and consumers and an example application to aerobic soil respiration. Geoscientific Model Development 10, 3277–3295.
Tang, J.Y., Riley, W.J., 2019. A theory of effective microbial substrate affinity parameters in variably saturated soils and an example application to aerobic soil heterotrophic respiration. Journal of Geophysical Research -Biogeosciences 124, 918–940.
van der Wal, A., de Boer, W., Smant, W., van Veen, J.A., 2007. Initial decay of woody fragments in soil is influenced by size, vertical position, nitrogen availability and soil origin. Plant and Soil 301, 189–201.
Vasconcelos, H.L., Laurance, W.F., 2005. Influence of habitat, litter type, and soil invertebrates on leaf-litter decomposition in a fragmented Amazonian landscape. Oecologia 144, 456–462.
Wang, B., Allison, S.D., 2019. Emergent properties of organic matter decomposition by soil enzymes. Soil Biology and Biochemistry 136, 107522.
Wang, G.S., Post, W.M., Mayes, M.A., 2013. Development of microbial-enzyme-mediated decomposition model parameters through steady-state and dynamic analyses. Ecological Applications 23, 255–272.
Wieder, W.R., Allison, S.D., Davidson, E.A., Georgiou, K., Hararuk, O., He, Y.J., Hopkins, F., Luo, Y.Q., Smith, M.J., Sulman, B., Todd-Brown, K., Wang, Y.P., Xia, J. Y., Xu, X.F., 2015. Explicitly representing soil microbial processes in Earth system models. Global Biogeochemical Cycles 29, 1782–1800.
Yeh, A.I., Huang, Y.C., Chen, S.H., 2010. Effect of particle size on the rate of enzymatic hydrolysis of cellulose. Carbohydrate Polymers 79, 192–199.
Zhu, Q., Riley, W.J., Tang, J., Koven, C.D., 2016. Multiple soil nutrient competition between plants, microbes, and mineral surfaces: model development, parameterization, and example applications in several tropical forests. Biogeosciences 13, 341–363.
Zhu, Q., Riley, W.J., Tang, J.Y., 2017. A new theory of plant-microbe nutrient competition resolves inconsistencies between observations and model predictions. Ecological Applications 27, 875–886.

Competitor and substrate sizes and diffusion together define enzymatic depolymerization and microbial substrate uptake rates

Tang, Jinyun; Riley, William J.

01 mingxi zhang Page 1
2/8/2023 3:24

02 mingxi zhang Page 1
2/8/2023 3:25

03 mingxi zhang Page 1
2/8/2023 3:27

04 mingxi zhang Page 2
2/8/2023 3:31

05 mingxi zhang Page 2
2/8/2023 3:27

06 mingxi zhang Page 2
2/8/2023 3:29

07 mingxi zhang Page 2
2/8/2023 3:31